Experimental evidence of plastic particles transfer at the water-air interface through bubble bursting

Maria Masry, Stéphanie Rossignol, Brice Temime Roussel, David Bourgogne, Pierre-Olivier Bussière, Badr R'mili, Pascal Wong-Wah-Chung

Experimental evidence of plastic particles transfer at the water-air interface through bubble bursting

Maria Masry [a], Stephanie Rossignol [a, *], Brice Temime Roussel [a], David Bourgogne [b], Pierre-Olivier Bussiere [b], Badr R'mili [a], Pascal Wong-Wah-Chung [a]

[a] *Aix Marseille Univ, CNRS, LCE, Marseille, France*

[b] *Universite Clermont Auvergne, CNRS, UMR 6296, Universite Blaise Pascal, Institut de Chimie de Clermont-Ferrand (ICCF), 8 Avenue Blaise Pascal, TSA 60026, CS 60026, 63178, Aubiere, Cedex, France*

Abstract

Plastic debris in the marine environment are the subject of an extensive literature. According to studies dedicated to the determination of plastic litter abundance and to the characterisation of degradation and fragmentation processes, models were used to estimate the global plastic debris abundance and to simulate their transfer and distribution. Despite these efforts, there is still missing plastic in the models used as areas exist where plastic abundance is less than that estimated. In parallel, microplastics presence in the atmosphere and in remote areas was confirmed suggesting long range atmospheric transport. Potentially addressing both these issues, recent literature suggests that microplastics (MPs) and nano- plastics (NPs) can be transferred from the marine environment to the atmosphere via the bursting of air bubbles at the sea surface. Nevertheless, to date there is no direct evidence of this transfer. In this study, we evaluate plastic particles transfer as a function of MPs/NPs characteristics and water composition by simulating the bubble bursting phenomenon in a laboratory reactor. Size distribution of transferred particles were recorded, and their plastic nature was confirmed using electron microscopy. Results show that under tested conditions, the transfer is possible but limited to particles smaller than 1 mm. The influence of the presence of proxies of components of the sea surface microlayer in the water was evaluated showing a higher particle transfer rate in the presence of a surfactant (sodium dodecyl sulfate) and no significant effect of polysaccharides (xanthan gum and dextran). The surface state of the particles can alter their behaviour in the aqueous phase and thus their transfer to the atmosphere. The effect of bubble size was also evaluated showing a higher transfer rate with the smaller bubble size. In addition, experiments performed with grounded polyethylene (PE) samples showed higher transfer for UV-aged PE than for pristine PE.

Keywords: Bubble bursting; Nano-plastic; Water-air interface; Transfer Surfactant

1. Introduction

The plastic industry witnessed an increase in plastic production that led to an increase in the amount of plastic waste dumped in landfills. It is estimated that by 2050 the humankind would have generated 33,000 million metric tons (Mt) of plastic waste of which 12,000 million Mt would be in dumps, landfills, and the natural environment (Geyer, 2020; Plastics Europe, 2019).

In the natural environment, these plastic debris are exposed to several factors especially sunlight and mechanical stress that can induce photodegradation and plastics fragmentation, leading to the formation of microplastics (MPs < 5 mm) and nanoplastics (NPs < 1 mm) (Andrady, 2017; Gigault et al., 2016; ter Halle et al., 2017, 2016). These plastic debris can be transferred from terrestrial into marine environment by rivers, drainage systems or hu- man activity (Auta et al., 2017; Barnes et al., 2009; Browne et al., 2011; Li et al., 2016; Peng et al., 2020). NPs and MPs are considered as hazardous materials that can contain toxic contaminants and their ecotoxicological impact on marine organisms is documented in numerous studies (Avio et al., 2017; Wright and Kelly, 2017).

Several models were used to estimate the global plastic debris abundance in the marine environment and to simulate its transfer and distribution (Jambeck et al., 2015; Koelmans et al., 2017; Maximenko et al., 2012; van Sebille et al., 2015; Wichmann et al., 2019). Jambeck et al., (2015) estimated that in 2010 between 4.8 and 12.7 million Mt of plastic entered the ocean from coastal environments while Eriksen et al., (2014) and Van Sebille et al., (2015) estimated that more than 5 trillion plastic pieces afloat at sea weighing over than 93,000 Mt (Eriksen et al., 2014; Jambeck et al., 2015; van Sebille et al., 2015). Several studies also used advanced technological means to determine the abundance of plastic litter (Mace, 2012; Moy, 2018). Despite these studies, there is still missing plastic in the models used in areas where plastic abundance is less than that estimated by the models (Wichmann et al., 2019). Thus, there are yet unknown factors, beside the unanalysed nano- fraction, that are not considered in these models and there is still no definitive answer to the negative mass balance of entering vs detected marine plastic debris.

In parallel, MPs are found in remote locations such as the French Pyrenees, the Swiss Alps, the Tibet Plateau or even the Arctic (Allen et al., 2019; Bergmann et al., 2019; Jiang et al., 2019; Zhang et al., 2016). MPs are also detected in dry and/or wet atmospheric deposition in urban and remote areas including in marine environments (Allen et al., 2020; Liu et al., 2019). This strongly suggests long range atmospheric transport of MPs that could be even more important for NPs due to longer atmospheric residence time for smaller particles (Allen et al., 2019; Bergmann et al., 2019; Bianco and Passananti, 2020; Zhang et al., 2019, 2020). Understanding fluxes of MPs and NPs between the atmosphere and the other environmental compartments appears thus of crucial importance to estimate the MPs and NPs burden of the atmosphere and the importance of atmospheric transport in the MPs-NPs global issue. It is also worth to note that, even though there is a limited number of studies concerning environmental exposure, airborne MPs and NPs are considered as a threat to human health (Gasperi et al., 2018; Prata, 2018).

Closely related to both these considerations, it was recently suggested that plastic particles can be transferred from the ocean surface to the atmosphere (Allen et al., 2020; Trainic et al., 2020; Zhang et al., 2020). One of the most likely scenarios of MPs and NPs sea to air transfer is via the bursting of air bubbles at the sea surface following wind stress and waves breaking. When an air bubble bursts at the air-water interface, two main phenomena occur: (i) the bursting of the bubble-cap film ejects droplets called "film drops" and (ii) the collapse of the remaining bubble cavity at the water surface expels droplets called "jet drops" (Kientzler et al., 1954). The bubble bursting is the subject of an extensive litera- ture concerning the formation of sea spray aerosol and the transfer of large amount of sea salt, organic matter and microorganisms

from the sea surface to the atmosphere (for instance (Bigg and Leck, 2008; Frossard et al., 2019; Fuentes et al., 2010; Meskhidze et al., 2019; O'Dowd and de Leeuw, 2007; Prather et al., 2013; Quinn et al., 1975; Wang et al., 2017). The composition of sea spray aero- sol is known to be influenced by the composition of the sea surface microlayer (SML) that is enriched in organic matter compared to the underlying water and can also accumulated MPs and potentially NPs (Anderson et al., 2018; Chae et al., 2015; Engel et al., 2017; Song et al., 2014; Thornton et al., 2016; Uning et al., 2018; Wurl et al., 2010).

In recent studies by Allen et al. (2020) and Trainic et al. (2020), air masses from coastal and marine atmospheres were sampled for microplastics suggesting that the detected MPs originate from the ocean. In the present work, the water-air transfer of MPs and/or NPs by the bubble bursting is evaluated in controlled laboratory conditions. The approach used consists of simulating the air bubble bursting at the surface of a water of known composition spiked with MPs or NPs. The size distribution of the air transferred particles is recorded according to sizes and types of MPs/NPs, water composition and bubbles size.

2. Materials and methods

2.1. Bubble bursting experimental setup

The experimental setup, presented in Fig. 1, consists of a glass cylindrical reaction vessel (capacity 10 L, height 430 mm, Lab. Flange 200, outer diameter 215 mm, inner diameter 200 mm) covered with a two-neck flat flange lid with an O-ring seal and a clamp to ensure sealing. This set was obtained from Lenz Laborglas GmbH & Co. KG. The two necks of the lid were sealed with precision seal rubber septa pierced in the middle to allow the entry of a Teflon inlet and metal outlet air lines. The reaction vessel was filled with 4 L of ultrapure water filtered at 0.2 mm with a resistivity of
18.2 MU cm purified by a Millipore device (Direct-Q® 5 UV)
equipped with a UV lamp (254 nm). This resulted in a water depth of approximately 120 mm.

Particle free air was generated by a Scroll Air class zero compressor and a zero-air generator Sonimix 3057. It was then pumped through the Teflon inlet air line entering the reactor. A mass flow controller (MFC) was used to control the flow rate of the air entering the reactor. This flow rate was fixed at 2.5 L/min.

Bubbles were generated in the water bulk by injecting particle free air through a porous material maintained in a stainless-steel support connected to the inlet air line and placed at the bottom of the reactor. In this study, porous material used were a sintered glass frit with a porosity grade 3 and a 100 mm diameter (VWR International, LLC) and a wire mesh with a 125 mm mesh and a 100 mm diameter (GKD Gebr. Kufferath AG). The stainless-steel support was custom made by SAFM - Localicsol (France). The porous material was placed in the support between two nitrile rubber O-rings and covered with an O-shaped retaining stainless- steel ring tightened on the support with nut clamping screws.

The aerosol generated via the bubbling passes then through the metal outlet sampling line. The entry of the sampling line is fixed at 300 mm above the water surface. Transferred particles were dried by a silica diffusion dryer placed on the sampling line before counting using a GRIMM optical particle counter (OPC). The OPC draws air with a flow rate of 1.2 L/min and provide particles size distribution between 0.250 and 32 mm (31 channels) with a frequency of 10 analysis per minute. The details of the measured channels are presented in the supplementary material S1. A vent was placed on the sampling line before the dryer to evacuate excess air pressure. The vent flow was monitored constantly using a flowmeter 4100 series from TSI Instruments (U.S.A.) to ensure that there is no air leak.

The particle transfer was verified by transmission electron microscopy (TEM), as an additional sampling of the generated aerosol was carried out by TEM grid filtration thanks to an MPS (R'mili et al., 2013). This sampling line was fixed on a T connector placed between the dryer and the OPC. The sampling TEM grid is a copper Quantifoil 1.2/1.3400 mesh from Agar Scientific®. The sampling flow rate was fixed at 0.3 L/min and was monitored by a flowmeter and regulated by a flow regulator valve and pump. The sampling was carried out for 90 min. TEM analysis were carried out on JEOL 2010 transmission microscope with a GATAN Ultrascan 1000XP (2k x 2k) camera and coupled with energy-dispersive X-ray spectroscopy (EDX).

2.2. Materials

Sodium dodecyl sulfate (SDS) (>99% pure) and xanthan gum were from Sigma-Aldrich and dextran (Clinical grade, MW 200,000e300,000) was from MP Biomedicals, LLC.

In this study, polystyrene particles of 350 ± 6 nm (PS 350 nm) and 600 ± 9 nm (PS 600 nm) in aqueous suspension, both at 1% solid concentration, were acquired from Thermo Scientific™ 3000 Series Nanosphere™ (size distribution < 3%). Polystyrene particles of 1.046 ± 0.016 mm (PS 1 mm) in aqueous suspension were acquired from microparticles GmbH (size distribution 3.4%). Each size stan- dard was exposed to ultrasound for 15 min before each experiment to ensure particle dispersion. Polyethylene nanospheres (PE_{Nano}) were obtained from Cospheric LLC as dry powder with a size distribution ranging from 200 to 9900 nm. For each experiment, 25.10^{-3} g of PE_{Nano} was suspended in 10 mL of water in a glass vial exposed to 15 min of ultrasound.

Bubble bursting experiments were also performed with two formulations of pristine and UV-aged PE. The formulations used were: (i) virgin PE containing a low level of stabilizers, and (ii) formulated PE containing 0.2% of Chimassorb 81 (anti-UV, BASF France), 0.2% of Irganox 1010 (antioxidant, BASF France) and 15% of Omyalite 90 (mineral filler, OMYA SAS France). Initial virgin PE pellets were supplied by SABIC® LLDPE 324CE and were then mixed with the additives in a Brabender mixer to make the formulated PE pellets using a Lescuyer granular. The pellets were hot pressed at 140 °C and 150 bars for 1 min using a Darragon press into films about 100 mm in diameter and 200 mm thick. Some of the PE films were exposed to UV in a SEPAP 12/24 (Atlas) accelerated artificial photo-aging chamber (4 medium pressure mercury vapor lamps, λ > 295 nm, 60 °C). The acceleration factor ranges between 10 and 15 compared to natural weathering in centre France (Lacoste et al., 2010). The virgin PE was exposed for 400 h while the formulated PE was exposed to 311 h, which resulted in the same oxidation degree for both formulations. The oxidation degree cor- responds to the photodegradation products formed during UV
exposure. Aged films were characterized by infrared spectroscopy in transmission mode (Supplementary material S2 and S3). Then pristine and aged films were cryo-milled into particles smaller than 1 mm using a Retsch Centrifugal Grinding Mill ZM 1000. Finally, 1 g of each pristine and aged PE of each formulation were tested sequentially in the reactor to evaluate particle transfer.

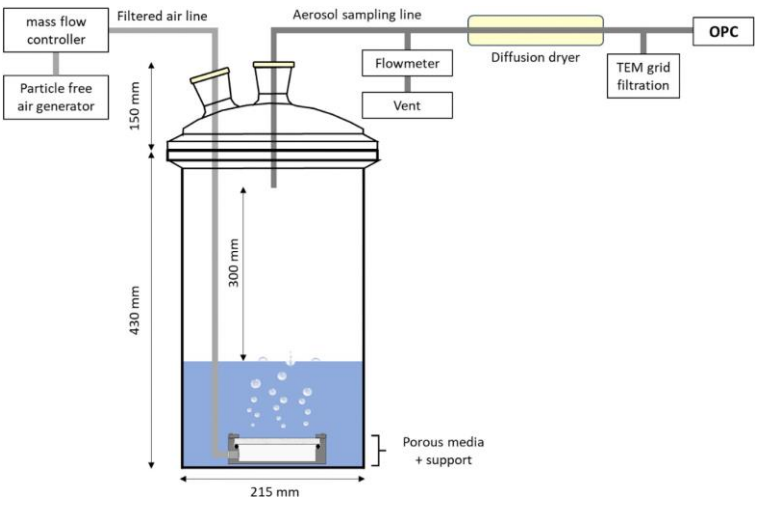

Fig. 1. Schematic view of the bubble bursting experimental setup.

2.3. Experiments

Before each experiment, the reactor was cleaned, rinsed, and filled with 4 L of ultrapure water. The system was then closed and purged with particle free air entering through the bubbling system for 20 min. Then, according to each experiment, surfactant and/or polysaccharides, and particles were added to the ultrapure water. To avoid counting particles in a destabilized system while adding, the first 10 min after each addition were not taken into account. The OPC was used to monitor the purging and to acquire the back- ground signal. A background signal of 10 min was considered for each experiment independently as it consisted of ultrapure water with the added concentration of surfactants and/or polysaccharides.

The experiments were limited to the use of ultrapure water instead of reconstituted seawater to avoid interferences in the measurements caused by salt crystals. Since salt crystals can alter the generated aerosol causing more interferences and complications in the background signal that might not allow us to detect a significant increase in the signal recorded after plastic particles addition.

3. Results and discussion

3.1. Transfer according to particle size

To determine particle sizes that are more likely to be transferred by bubble bursting into the atmosphere, after the purge and system equilibration 5 drops of PS particle standard of different sizes, 350 nm, 600 nm, and 1 mm were added to ultrapure water in independent experiments. The experiment was also performed with 25.10^{-3} g of PE_{Nano} suspended in water covering a size range from 200 to 9900 nm.

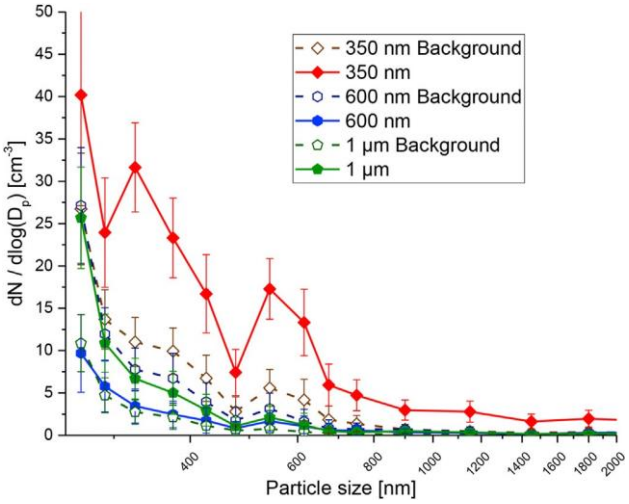

Fig. 2. Normalized mean particle size distribution measured by the OPC following PS particle addition into ultrapure water. Closed symbols represent the averaged signal for 20 min following particle addition and signal stabilisation. Open symbols represent the averaged background signal acquired for 10 min with ultrapure water right before particle addition.

Fig. 2 shows the normalized particle concentrations dN/dlog (Dp) (cm^{-3}) as a function of particle size (nm) according to OPC measurement channels, with dN being the total concentration of particles in a given channel and dlog (Dp) being the width of this channel.

As presented in Fig. 2, for 600 nm and 1 μm PS, no significant difference was observed between the background signal and the signal following particle addition, meaning that no particle transfer is observed. However, the distribution profile obtained after the addition of 350 nm PS particles clearly shows that particles of 350 nm are transferred to the atmosphere as single particles or as agglomerates.

Even though PS particles are suspended in water, bigger particles tend to sink due to their specific gravity of 1.05 (25 °C). Thus, 350 nm PS are more likely to be dispersed in the whole water column and transported by bubbles to the water surface while 600 nm and 1 mm PS particles tend to sink in the water column despite the bubbling. Moreover, the cap film formed in ultrapure water when the bubble arrives at the air/water interface can be thinner than 600 nm and 1 mm PS, thus these particle sizes are less likely to be transferred via the bubble bursting.

As for polyethylene particles, when comparing the background signal to that generated after PE_{Nano} (200–900 nm) addition (C1), no significant particle transfer occurred (Supplementary material S4-A). This is probably due to the hydrophobic nature of PE that tends to form agglomerates at the water surface making them less likely to be present in the bubble cap during the bursting.

3.2. Transfer according to water composition and particle properties

The effect of water composition was tested on both PS 350 nm and PE_{Nano} transfer in ultra-pure water and in the presence of surfactant and/or polysaccharides using the sintered glass frit to produce bubbles. The presence of SDS was tested at two concentration levels, 0.43 and 8.67 μM. The effect of polysaccharides was evaluated in the presence of xanthan gum and dextran at respectively 300 μg/L and 150 μg/L in ultrapure water. The transfer was also evaluated in an environmental-like conditions in the simultaneous presence of SDS and both polysaccharides with 0.43 μM of SDS and 300 mg/L and 150 mg/L respectively of xanthan gum and dextran. The concentrations were chosen according to previous studies in which the SML composition was determined (Dreshchinskii and Engel, 2017; Huang et al., 2015; Robinson et al., 2019b; Roslan et al., 2010; Thornton et al., 2016).

After the background signal recording, particles were added at the first concentration level (C1) followed by an equilibration phase of 10 min and the recording of the signal of interest for 20 min. Then the initial particle concentration level was doubled by a sec- ond identical addition (C2) followed by an equilibration phase of 10 min and the recording of the signal of interest for 30 min. Thus, for each particle type, two concentration levels were tested (C1 and C2). For PS 350 nm, 5 initial drops were added followed by 5 more drops 30 min after the first addition. For PE_{Nano}, 25.10^{-3} g were initially suspended in water, followed by a second addition of 25.10^{-3} g 30 min after the first addition. The results are presented in Figs. 3 and 4. In all cases, the error bars represent the standard deviation of the measurement on the duration of the acquisition.

Considering the case in ultrapure water as previously mentioned, 350 nm PS particles can be transferred to the atmosphere since the normalized particle concentration increases in the size range between 300 and 350 nm from 11 to 32 cm^{-3} after the first PS addition and to 47 cm^{-3} after the second PS addition (supplementary material S4–B). An increase of the particle con- centration is also noted in sizes higher than 350 nm. This could be due to transferred PS particles surrounded with water microlayers of different thicknesses not removed in the dryer or even as ag- glomerates. In the case of PE_{Nano} in ultrapure water presented in supplementary material S4-A, no significant transfer is noticed for the two particles concentration levels in comparison to the back- ground signal.

In the presence of 0.43 mM of SDS, as presented in Fig. 3-A, the normalized particle concentration increases in the size range of 300–350 nm from 20 to 59 cm^{-3} after the first PS 350 nm addition and to 82 cm^{-3} after the second PS 350 nm addition. Unlike with ultrapure water where the transfer peaks in the size range of 300–350 nm and less transfer occurs in higher size ranges, the presence of 0.43 μM SDS causes the peak to shift to higher size ranges as the transfer peak occurs in the size range of 350–400 nm. This shift is more obvious in Fig. 3-B with the higher concentration of SDS of 8.67 mM, for which the particle transfer occurs mainly in the size range of 500–580 nm (49 cm^{-3}) after the first and second addition, while no significant difference is observed in the size range 300–350 nm. This is probably attributed to the adsorption of SDS onto the PS surface that can increase the apparent diameter of the PS particle, in addition to the already mentioned water coating and agglomerates (Brown and Zhao, 1993; Turner et al., 1999).

These results were further investigated by sampling the generated aerosol by TEM grid filtration. The grid was then analysed by TEM and the images are presented in Fig. 5. Fig. 5-A present the different case scenarios of PS particle transfer, as single particles are present as well as agglomerates of three or more PS particles. While in Fig. 5-B, with the higher SDS concentration, single spherical particles with a 600 nm diameter are present as well as bigger agglomerates suggesting that PS particles are transferred coated by an SDS layer. The nature of this layer was confirmed by EDX analysis by the presence of the sulphur atom (supplementary material S5). Concerning the agglomerates transferred with 0.43 mM of SDS, the images 5-C and 5-D shows that these agglomerates can be transferred with or without SDS coating. This suggests that ag- glomerates can be transferred by both film and jet drops as the chemical composition and organic volume fraction is known to differ between particles generated from film and jet drops (Wang et al., 2017). Film drops transport organic species concentrated in the SML, in our case SDS. This suggest that the agglomerate coated by an SDS layer in Fig. 5-D was more likely transferred by film drop, while the agglomerate in Fig. 5-C was more likely surrounded by a water layer that dried, thus was most probably transferred by jet drops.

The effect of 0.43 and 8.67 μM of SDS was also evaluated on PE_{Nano} particles and is presented respectively in Fig. 4-A and 4-B. In both cases the transfer was more remarkable in the size range between 350 and 650 nm. The presence of 0.43 μM of SDS increases the normalized particle size of approximately 22 cm^{-3} in each channel of the OPC between 350 and 580 nm while the presence of 8.67 mM of SDS increases the particle concentration of approximately 388 cm^{-3} between 350 and 400 nm, and 321 cm^{-3} between 500 and 580 nm. No significant increase was noticed with 0.43 μM of SDS, while in the case of 8.67 mM an increase of between 140 and 192 cm^{-3} was noted from 250 to 350 nm suggesting that SDS can stabilize PE_{Nano} present preventing some from agglomeration.

Unlike the case of PS, the second addition of PE_{Nano} does not lead to an increase in the number of particles generated. This could be explained by the different behaviour of PS and PE_{Nano} particles in water, as suggested by the temporal evolution of the normalized particle concentration measured in the 300–350 nm channel of the OPC in supplementary material S6. Transferred particle concentration

increases and then stabilises following the first and second addition of PS to water, while for PE_{Nano} this concentration in- creases directly after both additions and then decreases. Since PS particles remain suspended in the water, the number of PS particles transferred remains stable after each addition, while PE_{Nano} hydrophobic particles tend to agglomerate leading to a decrease in the number of free particles present in the water as a function of time as well as in the number of particles transferred to the atmosphere. In the presence of polysaccharides, xanthan gum and dextran, Fig. 3-C and 4-C respectively show that the particle concentrations are equivalent to those obtained in ultrapure water for both for PS and PE_{Nano} particles showing no significant effect of the presence of polysaccharides on particle transfer. PS particles transfer rate was the same in ultrapure water and in the presence of polysaccharides while PE_{Nano} particles did not transfer in both mediums.

Fig. 3-D shows the results in the presence of 0.43 µM of SDS,
300 µg/L of xanthan gum, and 150 µg/L of dextran. The mean par- ticle size distribution after the first addition of PS 350 nm particles shows no significant difference than that in the case of only 0.43 mM of SDS in Fig. 3-A. But in the presence of SDS, xanthan gum, and dextran, no significant effect was noticed between the two con- centration levels of PS. This finding needs more investigation. The same effects are noticed in the case of PE_{Nano} in the presence of SDS and polysaccharides presented in Fig. 4-D. The mean size distribution shows no significant difference to that obtained with only 0.43 µM of SDS in Fig. 4-A and between the two concentration levels of PE_{Nano}.

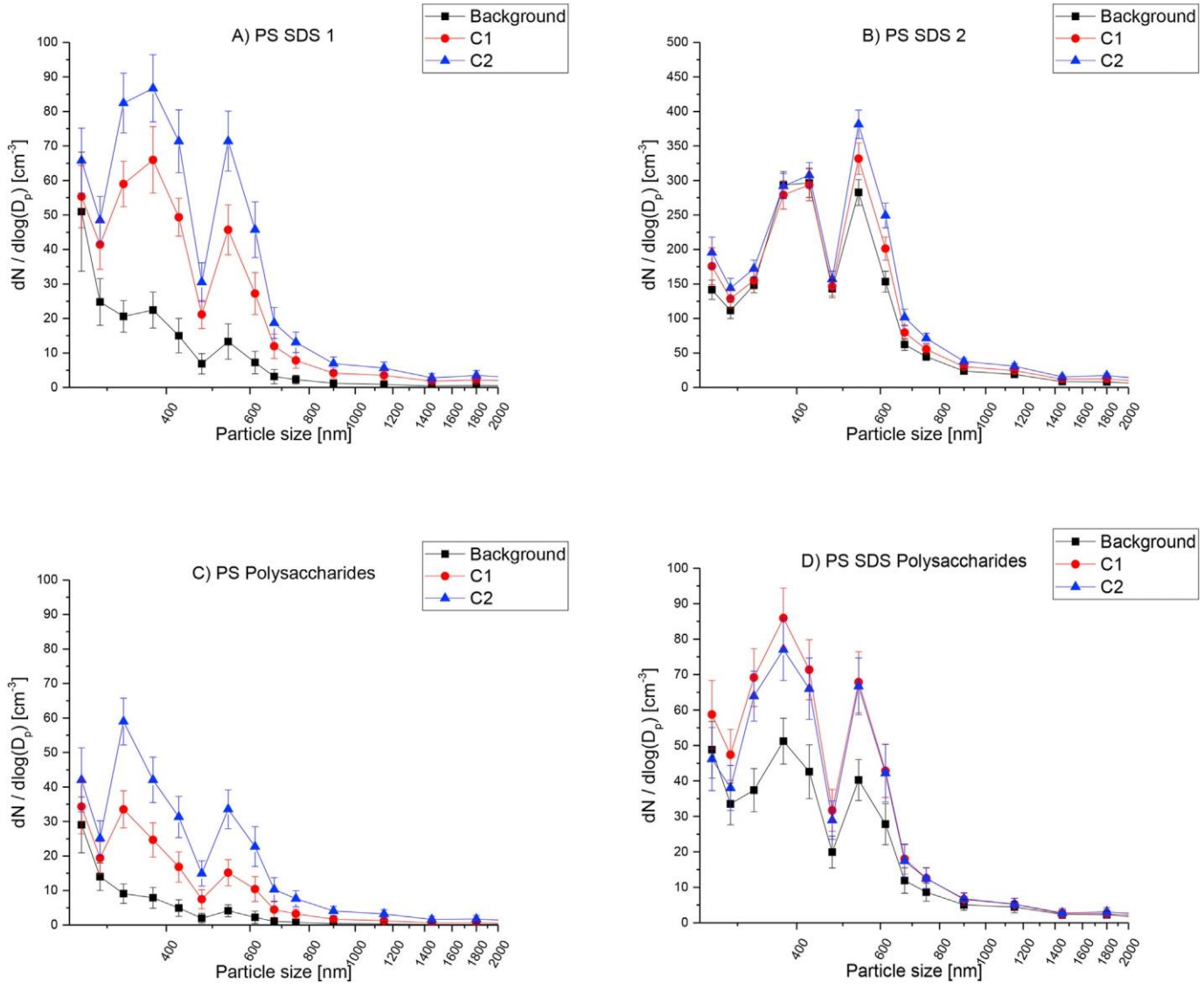

Fig. 3. Normalized mean particle size distribution for the background signal and two concentration levels of PS 350 nm measured by the OPC in different water composition: (A) water þ SDS 0.43 mM; (B) water þ SDS 8.67 mM; (C) water þ xanthan gum 300 mg/L þ dextran 150 mg/L; and (D) water þ SDS 0.43 mM þ xanthan gum 300 mg/L þ dextran 150 mg/L.

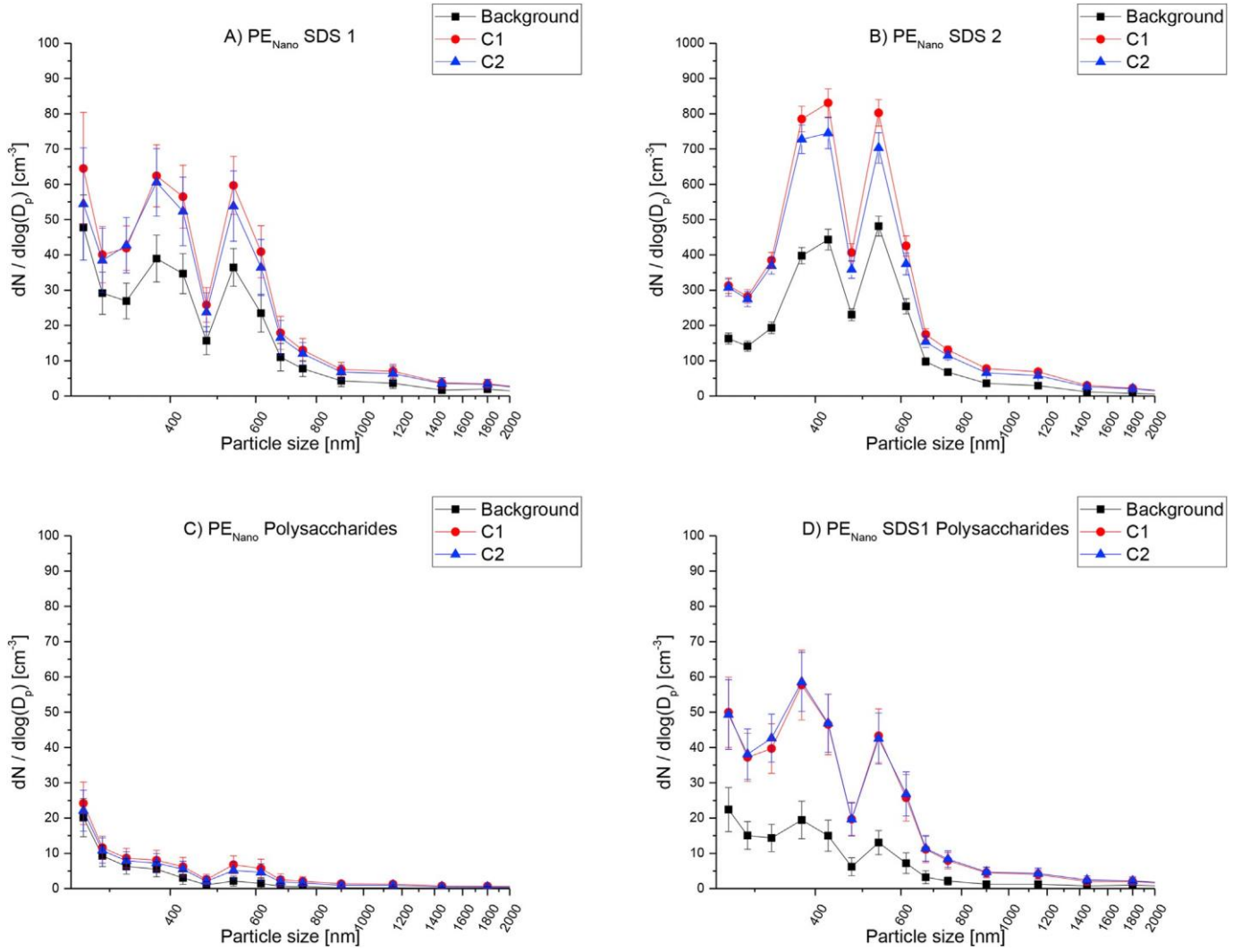

Fig. 4. Normalized mean particle size distribution for the background signal, and two concentration levels of PE$_{Nano}$ (200e9900 nm) measured by the OPC in different water composition: (A) water þ SDS 0.43 mM; (B) water þ SDS 8.67 mM; (C) water þ xanthan gum 300 mg/L þ dextran 150 mg/L; and (D) water þ SDS 0.43 mM þ xanthan gum 300 mg/ L þ dextran 150 mg/L.

3.3. Transfer according to bubble size

To evaluate the effect of bubble size on particle transfer, two porous materials were used to produce different bubble sizes: (i) a sintered glass frit (porosity 3) and (ii) a wire mesh with a 125 µm mesh size. The porosity 3 sintered glass frit was used to produce a bubble size range below the Hinze scale and theoretically similar to that produced by natural wave breaking. While the wire mesh was used to test a bubble size range set above the Hinze scale and that can also occur naturally in wave breaking (Crawford and Farmer, 1987; Deane and Stokes, 2002; Johnson and Cooke, 1979; Robinson et al., 2019a; Sellegri et al., 2006). The bubble size range is evaluated according to results by Robinson et al. (2019a) that used glass frits with similar porosities to those used in this study to produce bubbles with size ranges occurring below (smaller pores) and above (larger pores) the Hinze scale. Since SDS solution was proven to promote particle transfer compared to ultrapure water, SDS was added to the water at 0.43 µM. Since the concentrations of SDS used in this study is lower than the critical micelle concentration (8.2 mM), the effect of SDS on the bubble size distribution and aerosol production is considered limited (Sellegri et al., 2006; Xu et al., 2009).

The effect of bubble sizes was evaluated on both PS 350 nm and PE$_{Nano}$ (200-9900 nm). Then either 5 drops of PS 350 nm or 25.10^{-3} g of PE$_{Nano}$ suspended in water were added, and the signal was recorded for 10 min. Results are presented in supplementary material S7. The number of particles transferred with the wire mesh via the bubble bursting for both PS and PE$_{Nano}$ was much less than that transferred by the glass frit that produced more smaller bubbles.

Although the wire mesh with 125 µm pore size produced larger bubbles than those produced by the glass frit with smaller pore size (16 and 40 mm), it produced bigger but fewer bubbles giving that the entering air flow rate was kept constant at 2.5 L/min. Even though larger bubbles produce wider jets, smaller bubbles produce multiple jet droplets and promotes organic compounds transfer from the water surface to the atmosphere (Ghabache and Seon, 2016; Keene et al., 2007; Mead-Hunter et al., 2018). Thus, smaller bubbles tend to produce multiple jet drops increasing the probability of particle transfer.

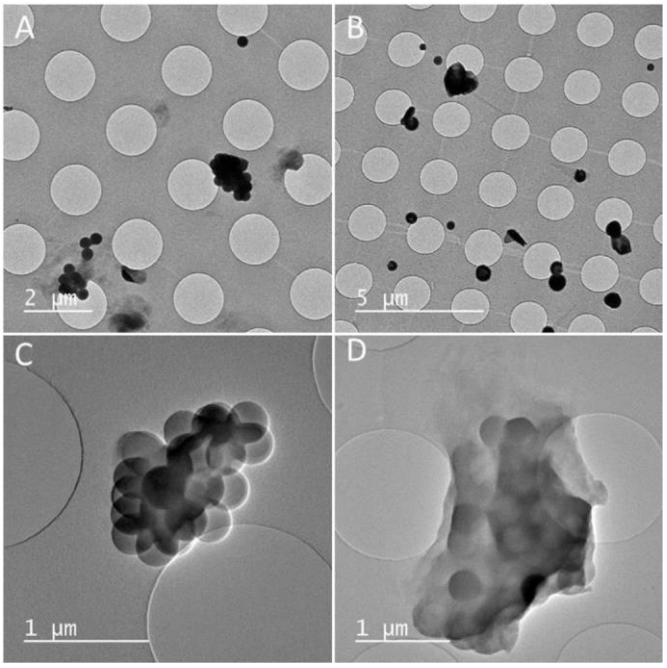

Fig. 5. TEM images of PS 350 nm particles sampled from (A) water þ SDS 0.43 mM and (B) water þ SDS 8.67 mM; and agglomerates transferred in the presence of 0.43 mM of SDS (C) agglomerate and (D) agglomerate surrounded with an SDS layer.

3.4. Transfer of PE exposed to UV

To evaluate the effect of plastic photodegradation in the marine environment on their transfer to the atmosphere, bubble bursting experiments were performed with two different formulations of pristine and UV aged PE.

Environmental concentrations of surfactants and poly- saccharides were added to the water, at 0.43 µM for SDS and 300 µg/L and 150 µg/L respectively for xanthan gum and dextran. Then the average number of particles generated for 30 min after PE addition is acquired.

As presented in Fig. 6-A for virgin PE, no significant difference is noticed between the signals generated by the pristine virgin PE and the background. In the case of the UV aged PE, particles smaller than 500 nm are clearly transferred from the water surface to the atmosphere. This shows that UV exposure and mechanical force not only can induce plastics fragmentation, as proven in the literature, but also generate nanometric fragments that can be transferred to the atmosphere via bubble bursting (Song et al., 2017; ter Halle et al., 2016). The behaviour of PE particles generated after UV exposure in the water resembles that of the PS ones as the oxidation of the PE particles surface due to the formation of oxygenated groups makes it less hydrophobic. So UV aged PE particles does not tend to agglomerate unlike hydrophobic PE_{Nano} (supplementary material S8) (Gardette, 1993; Rouillon et al., 2016).

On the other hand, a slight increase is noticed for both pristine and UV aged formulated PE compared to the background signal (Fig. 6-B). However, we observe the same increase in the number of particles following the addition of PE regardless of its weathering degree. The lack of particle transfer can also be due to the presence of 15% of calcium carbonate in the formulated PE making it denser than water and thus more subject to sinking compared to virgin PE that floats at the water surface. Thus, plastics fragmentation and generated particles transfer depends on the initial plastics formulation and nature as well as their surface oxidation state.

4. Conclusions

In this work the effects of water composition, bubble size, particles type and size on plastic particles transfer were evaluated by simulating the bubble bursting phenomenon in a laboratory reactor and sampling the atmosphere using an OPC and TEM grids. Particle transfer from water surface to the atmosphere is proven to be possible through bubble bursting, and obviously more significant for smaller nanometric particles. The presence of SDS induced higher transfer rate while the presence of polysaccharides had no effect. In real environmental conditions, the transfer may also depend on the composition of the SML, the types and concentrations of the present surfactants, as well as the salinity of the water which facilitates plastic particles flotation. The transfer was highly affected with the surface state of the particle as hydrophobic particles tends to agglomerate lowering the transfer rate while particles with more hydrophilic surface were in suspension in water and more easily transferred. A higher transfer rate of particles was established with smaller bubbles compared with bigger ones for identical air flow rate. UV exposure and mechanical force induced the fragmentation of PE and generated particles transferred via bubble bursting into the atmosphere.

In future work, it will be interesting to quantify plastic particles transfer rate as it can bring an answer to the missing plastic in marine models and to the significance of the bubble bursting as a source for atmospheric plastic particles.

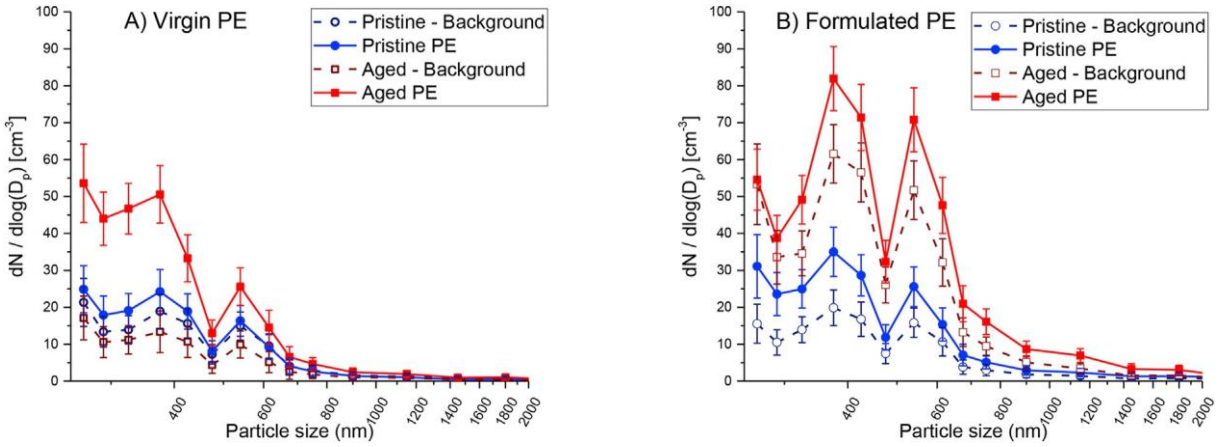

Fig. 6. Normalized mean particle size distribution of the background signals, pristine, and UV aged (A) virgin PE and (B) formulated PE.

Acknowledgment

The authors would like to thank Jean-François LARCHE and Nexans for providing pristine virgin and formulated polyethylene, and team POPPI from the "Institut de Chimie de Clermont-Ferrand" for the photodegradation of PE samples. The authors would also like to thank the CINaM (Centre Interdisciplinaire de Nanoscience de Marseille), especially Damien Chaudanson and Alexandre Altie for TEM images.

References

Allen, S., Allen, D., Moss, K., Le Roux, G., Phoenix, V.R., Sonke, J.E., 2020. Examination of the ocean as a source for atmospheric microplastics. PloS One 15, e0232746. https://doi.org/10.1371/journal.pone.0232746.

Allen, S., Allen, D., Phoenix, V.R., Le Roux, G., Durantez Jimenez, P., Simonneau, A., Binet, S., Galop, D., 2019. Atmospheric transport and deposition of microplastics in a remote mountain catchment. Nat. Geosci. 12, 339e344. https://doi.org/ 10.1038/s41561-019-0335-5.

Anderson, Z.T., Cundy, A.B., Croudace, I.W., Warwick, P.E., Celis-Hernandez, O., Stead, J.L., 2018. A rapid method for assessing the accumulation of microplastics in the sea surface microlayer (SML) of estuarine systems. Sci. Rep. 8 https:// doi.org/10.1038/s41598-018-27612-w.

Andrady, A.L., 2017. The plastic in microplastics: a review. Mar. Pollut. Bull. 119, 12e22. https://doi.org/10.1016/j.marpolbul.2017.01.082.

Auta, H.S., Emenike, C.U., Fauziah, S.H., 2017. Distribution and importance of microplastics in the marine environment: a review of the sources, fate, effects, and potential solutions. Environ. Int. 102, 165e176. https://doi.org/10.1016/j.envint.2017.02.013.

Avio, C.G., Gorbi, S., Regoli, F., 2017. Plastics and microplastics in the oceans: from emerging pollutants to emerged threat. Mar. Environ. Res. 128, 2e11. https:// doi.org/10.1016/j.marenvres.2016.05.012.

Barnes, D.K.A., Galgani, F., Thompson, R.C., Barlaz, M., 2009. Accumulation and fragmentation of plastic debris in global environments. Phil. Trans. R. Soc. B 364, 1985e1998. https://doi.org/10.1098/rstb.2008.0205.

Bergmann, M., Mützel, S., Primpke, S., Tekman, M.B., Trachsel, J., Gerdts, G., 2019. White and wonderful? Microplastics prevail in snow from the Alps to the arctic. Sci. Adv. 5, eaax1157 https://doi.org/10.1126/sciadv.aax1157.

Bianco, A., Passananti, M., 2020. Atmospheric micro and nanoplastics: an enormous microscopic problem. Sustainability 12, 7327. https://doi.org/10.3390/ su12187327.

Bigg, E.K., Leck, C., 2008. The composition of fragments of bubbles bursting at the ocean surface. J. Geophys. Res. 113, D11209. https://doi.org/10.1029/ 2007JD009078.

Brown, W., Zhao, J., 1993. Adsorption of sodium dodecyl sulfate on polystyrene latex particles using dynamic light scattering and zeta potential measurements. Macromolecules 26, 2711e2715. https://doi.org/10.1021/ma00063a012.

Browne, M.A., Crump, P., Niven, S.J., Teuten, E., Tonkin, A., Galloway, T., Thompson, R., 2011. Accumulation of microplastic on shorelines woldwide: sources and sinks. Environ. Sci. Technol. 45, 9175e9179. https://doi.org/10.1021/es201811s.

Chae, D.-H., Kim, I.-S., Kim, S.-K., Song, Y.K., Shim, W.J., 2015. Abundance and dis- tribution characteristics of microplastics in surface seawaters of the incheon/ kyeonggi coastal region. Arch. Environ. Contam. Toxicol. 69, 269e278. https:// doi.org/10.1007/s00244-015-0173-4.

Crawford, G.B., Farmer, D.M., 1987. On the spatial distribution of ocean bubbles. J. Geophys. Res. 92, 8231. https://doi.org/10.1029/JC092iC08p08231.

Deane, G.B., Stokes, M.D., 2002. Scale dependence of bubble creation mechanisms in breaking waves. Nature 418, 839e844. https://doi.org/10.1038/nature00967.

Dreshchinskii, A., Engel, A., 2017. Seasonal variations of the sea surface microlayer at the boknis eck times series station (baltic

sea). J. Plankton Res. 39, 943e961. https://doi.org/10.1093/plankt/fbx055.
Engel, A., Bange, H.W., Cunliffe, M., Burrows, S.M., Friedrichs, G., Galgani, L., Herrmann, H., Hertkorn, N., Johnson, M., Liss, P.S., Quinn, P.K., Schartau, M., Soloviev, A., Stolle, C., Upstill-Goddard, R.C., van Pinxteren, M., Zäncker, B., 2017. the ocean's vital skin: toward an integrated understanding of the sea surface microlayer. Front. Mar. Sci. 4, 165. https://doi.org/10.3389/fmars.2017.00165.
Eriksen, M., Lebreton, L.C.M., Carson, H.S., Thiel, M., Moore, C.J., Borerro, J.C., Galgani, F., Ryan, P.G., Reisser, J., 2014. Plastic pollution in the world's oceans: more than 5 trillion plastic pieces weighing over 250,000 tons afloat at sea. PloS One 9, e111913. https://doi.org/10.1371/journal.pone.0111913.
Frossard, A.A., Long, M.S., Keene, W.C., Duplessis, P., Kinsey, J.D., Maben, J.R., Kieber, D.J., Chang, R.Y.-W., Beaupre, S.R., Cohen, R.C., Lu, X., Bisgrove, J., Zhu, Y., 2019. Marine aerosol production via detrainment of bubble plumes generated in natural seawater with a forced-air venturi. J. Geophys. Res. Atmos. 124, 10931e10950. https://doi.org/10.1029/2019JD030299.
Fuentes, E., Coe, H., Green, D., de Leeuw, G., McFiggans, G., 2010. Laboratory- generated primary marine aerosol via bubble-bursting and atomization. Atmos. Meas. Tech. 141e162.
Gardette, J.-L., 1993. MicroFTIR spectroscopic profiling of aged polymer films Spectroscopy Europe, 5, 28e32.
Gasperi, J., Wright, S.L., Dris, R., Collard, F., Mandin, C., Guerrouache, M., Langlois, V., Kelly, F.J., Tassin, B., 2018. Microplastics in air: are we breathing it in? Curr. Opin. Environ. Sci. Health. 1, 1e5. https://doi.org/10.1016/j.coesh.2017.10.002.
Geyer, R., 2020. Production, use, and fate of synthetic polymers. In: Plastic Waste and Recycling. Elsevier, pp. 13e32. https://doi.org/10.1016/B978-0-12-817880- 5.00002-5.
Ghabache, E., Seon, T., 2016. Size of the top jet drop produced by bubble bursting. Phys. Rev. Fluids 1, 051901. https://doi.org/10.1103/PhysRevFluids.1.051901.
Gigault, J., Pedrono, B., Maxit, B., Ter Halle, A., 2016. Marine plastic litter: the un- analyzed nano-fraction. Environ. Sci.: Nano 3, 346e350. https://doi.org/ 10.1039/C6EN00008H.
Huang, Y.-J., Brimblecombe, P., Lee, C.-L., Latif, M.T., 2015. Surfactants in the sea- surface microlayer and sub-surface water at estuarine locations: their concentration, distribution, enrichment, and relation to physicochemical characteris- tics. Mar. Pollut. Bull. 97, 78e84. https://doi.org/10.1016/j.marpolbul.2015.06.031.
Jambeck, J.R., Geyer, R., Wilcox, C., Siegler, T.R., Perryman, M., Andrady, A., Narayan, R., Law, K.L., 2015. Plastic waste inputs from land into the ocean. Mar. Pol. 347, 768e771.
Jiang, C., Yin, L., Li, Z., Wen, X., Luo, X., Hu, S., Yang, H., Long, Y., Deng, B., Huang, L., Liu, Y., 2019. Microplastic pollution in the rivers of the Tibet Plateau. Environ. Pollut. 249, 91e98. https://doi.org/10.1016/j.envpol.2019.03.022.
Johnson, B.D., Cooke, R.C., 1979. Bubble populations and spectra in coastal waters: a photographic approach. J. Geophys. Res. 84, 3761. https://doi.org/10.1029/ JC084iC07p03761.
Keene, W.C., Maring, H., Maben, J.R., Kieber, D.J., Pszenny, A.A.P., Dahl, E.E., Izaguirre, M.A., Davis, A.J., Long, M.S., Zhou, X., Smoydzin, L., Sander, R., 2007. Chemical and physical characteristics of nascent aerosols produced by bursting bubbles at a model air-sea interface. J. Geophys. Res. 112, D21202. https:// doi.org/10.1029/2007JD008464.
Kientzler, C.F., Arons, A.B., Blanchard, D.C., Woodcock, A.H., 1954. Photographic investigation of the projection of droplets by bubbles bursting at a water surface. Tellus 6, 1e7. https://doi.org/10.1111/j.2153-3490.1954.tb01085.x.
Koelmans, A.A., Kooi, M., Law, K.L., van Sebille, E., 2017. All is not lost: deriving a top- down mass budget of plastic at sea. Environ. Res. Lett. 12, 114028. https:// doi.org/10.1088/1748-9326/aa9500.
Lacoste, J., Lemaire, J., Siampiringue, N., 2010. Predicting the weathering of poly- meric materials within the mechanistic approach based on artificial accelerated and ultraaccelerated photoageing equipments. In: Presented at the 8th Inter- national Symposium on Weatherability, Tokyo.
Li, W.C., Tse, H.F., Fok, L., 2016. Plastic waste in the marine environment: a review of sources, occurrence and effects. Sci. Total Environ. 566e567, 333e349. https:// doi.org/10.1016/j.scitotenv.2016.05.084.
Liu, K., Wu, T., Wang, X., Song, Z., Zong, C., Wei, N., Li, D., 2019. Consistent transport of terrestrial microplastics to the ocean through atmosphere. Environ. Sci. Technol. 53, 10612e10619. https://doi.org/10.1021/acs.est.9b03427.
Mace, T.H., 2012. At-sea detection of marine debris: overview of technologies, processes, issues, and options. Mar. Pollut. Bull. 65, 23e27.
Maximenko, N., Hafner, J., Niiler, P., 2012. Pathways of marine debris derived from trajectories of Lagrangian drifters. Mar. Pollut. Bull. 65, 51e62. https://doi.org/ 10.1016/j.marpolbul.2011.04.016.
Mead-Hunter, R., Gumulya, M.M., King, A.J.C., Mullins, B.J., 2018. Ejection of droplets from a bursting bubble on a free liquid surfaceda dimensionless criterion for "jet" droplets. Langmuir 34, 6307e6313. https://doi.org/10.1021/acs.langmuir.8b00664.
Meskhidze, N., Salter, M., Sellegri, K., Elliott, S., 2019. Ocean contributions to the marine boundary layer aerosol budget. Atmosphere 10, 98. https://doi.org/ 10.3390/atmos10020098.
Moy, K., 2018. Mapping coastal marine debris using aerial imagery and spatial analysis. Mar. Pollut. Bull. 132, 52e59.
O'Dowd, C.D., de Leeuw, G., 2007. Marine aerosol production: a review of the cur- rent knowledge. Philos. Trans. A Math. Phys. Eng. Sci. 365, 1753e1774. https:// doi.org/10.1098/rsta.2007.2043.
Peng, L., Fu, D., Qi, H., Lan, C.Q., Yu, H., Ge, C., 2020. Micro- and nano-plastics in marine environment: source, distribution and threats d a review. Sci. Total Environ. 698, 134254. https://doi.org/10.1016/j.scitotenv.2019.134254.
Plastics Europe, 2019. Plastics - the Facts 2019.
Prata, J.C., 2018. Airborne microplastics: consequences to human health? Environ. Pollut. 234, 115e126. https://doi.org/10.1016/j.envpol.2017.11.043.
Prather, K.A., Bertram, T.H., Grassian, V.H., Deane, G.B., Stokes, M.D., DeMott, P.J., Aluwihare, L.I., Palenik, B.P., Azam, F., Seinfeld, J.H., Moffet, R.C., Molina, M.J., Cappa, C.D., Geiger, F.M., Roberts, G.C., Russell, L.M., Ault, A.P., Baltrusaitis, J., Collins, D.B., Corrigan, C.E., Cuadra-Rodriguez, L.A., Ebben, C.J., Forestieri, S.D., Guasco, T.L., Hersey, S.P., Kim, M.J., Lambert, W.F., Modini, R.L., Mui, W., Pedler, B.E., Ruppel, M.J., Ryder, O.S., Schoepp, N.G., Sullivan, R.C., Zhao, D., 2013. Bringing the ocean into the laboratory to probe

the chemical complexity of sea spray aerosol. Proc. Natl. Acad. Sci. Unit. States Am. 110, 7550e7555. https://doi.org/10.1073/pnas.1300262110.
Quinn, J.A., Steinbrook, R.A., Anderson, J.L., 1975. Breaking bubbles and the water- to-air transport of particulate matter. Chem. Eng. Sci. 30, 1177e1184. https:// doi.org/10.1016/0009-2509(75)87021-7.
R'mili, B., Le Bihan, O.L.C., Dutouquet, C., Aguerre-Charriol, O., Frejafon, E., 2013. Particle sampling by TEM grid filtration. AS&T 47, 767e775. https://doi.org/ 10.1080/02786826.2013.789478.
Robinson, T.-B., Giebel, H.-A., Wurl, O., 2019a. Riding the plumes: characterizing bubble scavenging conditions for the enrichment of the sea-surface microlayer by transparent exopolymer particles. Atmosphere 10, 454. https://doi.org/10.3390/atmos10080454.
Robinson, T.-B., Stolle, C., Wurl, O., 2019b. Depth is relative: the importance of depth on TEP in the NearSurface environment. Ocean Sci. 15, 1653e1666. https:// doi.org/10.5194/os-2019-79.
Roslan, R.N., Hanif, N.M., Othman, M.R., Azmi, W.N.F.W., Yan, X.X., Ali, M.M., Mohamed, C.A.R., Latif, M.T., 2010. Surfactants in the sea-surface microlayer and their contribution to atmospheric aerosols around coastal areas of the Malay- sian peninsula. Mar. Pollut. Bull. 60, 1584e1590. https://doi.org/10.1016/j.marpolbul.2010.04.004.
Rouillon, C., Bussiere, P.-O., Desnoux, E., Collin, S., Vial, C., Therias, S., Gardette, J.-L., 2016. Is carbonyl index a quantitative probe to monitor polypropylenephotodegradation? Polym. Degrad. Stabil. 128, 200e208. https://doi.org/10.1016/j.polymdegradstab.2015.12.011.
Sellegri, K., O'Dowd, C.D., Yoon, Y.J., Jennings, S.G., Leeuw, G. de, 2006. Surfactants and submicron sea spray generation. J. Geophys. Res. Atmos. 111 https://doi.org/ 10.1029/2005JD006658.
Song, Y.K., Hong, S.H., Jang, M., Han, G.M., Jung, S.W., Shim, W.J., 2017. Combined effects of UV exposure duration and mechanical abrasion on microplastic fragmentation by polymer type. Environ. Sci. Technol. 51, 4368e4376. https://doi.org/10.1021/acs.est.6b06155.
Song, Y.K., Hong, S.H., Jang, M., Kang, J.-H., Kwon, O.Y., Han, G.M., Shim, W.J., 2014. Large accumulation of micro-sized synthetic polymer particles in the sea sur- face microlayer. Environ. Sci. Technol. 48, 9014e9021. https://doi.org/10.1021/es501757s.
ter Halle, A., Ladirat, L., Gendre, X., Goudouneche, D., Pusineri, C., Routaboul, C., Tenailleau, C., Duployer, B., Perez, E., 2016. Understanding the fragmentation pattern of marine plastic debris. Environ. Sci. Technol. 50, 5668e5675. https://doi.org/10.1021/acs.est.6b00594.
ter Halle, A., Ladirat, L., Martignac, M., Mingotaud, A.F., Boyron, O., Perez, E., 2017. To what extent are microplastics from the open ocean weathered? Environ. Pollut. 227, 167e174. https://doi.org/10.1016/j.envpol.2017.04.051.
Thornton, D.C.O., Brooks, S.D., Chen, J., 2016. Protein and carbohydrate exopolymer particles in the sea surface microlayer (SML). Front. Mar. Sci. 3 https://doi.org/ 10.3389/fmars.2016.00135.
Trainic, M., Flores, J.M., Pinkas, I., Pedrotti, M.L., Lombard, F., Bourdin, G., Gorsky, G., Boss, E., Rudich, Y., Vardi, A., Koren, I., 2020. Airborne microplastic particles detected in the remote marine atmosphere. Commun Earth Environ 1, 64. https://doi.org/10.1038/s43247-020-00061-y.
Turner, S.F., Clarke, S.M., Rennie, A.R., Thirtle, P.N., Cooke, D.J., Li, Z.X., Thomas, R.K., 1999. Adsorption of sodium dodecyl sulfate to a polystyrene/water interface studied by neutron reflection and attenuated total reflection infrared spec- troscopy. Langmuir 15, 1017e1023. https://doi.org/10.1021/la980199h.
Uning, R., Latif, M.T., Yu, K.L., Cheng, S.Y., Ahamad, F., Khan, M.F., Bedurus, E.A., Suratman, S., 2018. Surfactants in the sea surface microlayer, underlying water and atmospheric particles of tropical coastal ecosystems. Water Air Soil Pollut. 229 https://doi.org/10.1007/s11270-018-3961-4.
van Sebille, E., Wilcox, C., Lebreton, L., Maximenko, N., Hardesty, B.D., van Franeker, J.A., Eriksen, M., Siegel, D., Galgani, F., Law, K.L., 2015. A global in- ventory of small floating plastic debris. Environ. Res. Lett. 10, 124006. https:// doi.org/10.1088/1748-9326/10/12/124006.
Wang, X., Deane, G.B., Moore, K.A., Ryder, O.S., Stokes, M.D., Beall, C.M., Collins, D.B., Santander, M.V., Burrows, S.M., Sultana, C.M., Prather, K.A., 2017. The role of jet and film drops in controlling the mixing state of submicron sea spray aerosol particles. Proc. Natl. Acad. Sci. U.S.A. 114, 6978e6983. https://doi.org/10.1073/pnas.1702420114.
Wichmann, D., Delandmeter, P., van Sebille, E., 2019. Influence of near-surface currents on the global dispersal of marine microplastic. J. Geophys. Res. Oceans 124, 6086e6096. https://doi.org/10.1029/2019JC015328.
Wright, S.L., Kelly, F.J., 2017. Plastic and human health: a micro issue? Environ. Sci. Technol. 51, 6634e6647. https://doi.org/10.1021/acs.est.7b00423.
Wurl, O., Wurl, E., Miller, L., Johnson, K., Vagle, S., 2010. Formation and distribution of sea-surface microlayers. Biogeosci. Discuss. 7, 5719e5755. https://doi.org/ 10.5194/bgd-7-5719-2010.
Xu, Q., Nakajima, M., Ichikawa, S., Nakamura, N., Roy, P., Okadome, H., Shiina, T., 2009. Effects of surfactant and electrolyte concentrations on bubble formation and stabilization. J. Colloid Interface Sci. 332, 208e214. https://doi.org/10.1016/j.jcis.2008.12.044.
Zhang, K., Su, J., Xiong, X., Wu, X., Wu, C., Liu, J., 2016. Microplastic pollution of lakeshore sediments from remote lakes in Tibet plateau, China. Environ. Pollut. 219, 450e455. https://doi.org/10.1016/j.envpol.2016.05.048.
Zhang, Y., Gao, T., Kang, S., Sillanpää, M., 2019. Importance of atmospheric transport for microplastics deposited in remote areas. Environ. Pollut. 254, 112953. https://doi.org/10.1016/j.envpol.2019.07.121.
Zhang, Y., Kang, S., Allen, S., Allen, D., Gao, T., Sillanpää, M., 2020. Atmospheric microplastics: a review on current status and perspectives. Earth Sci. Rev. 203, 103118. https://doi.org/10.1016/j.earscirev.2020.103118.

Supporting information

Experimental evidence of plastic particles transfer at the water-air interface through bubble bursting.

Maria Masry[a], Stéphanie Rossignol[a*], Brice Temime Roussel[a], David Bourgogne[b], Pierre-Olivier Bussière[b], Badr R'mili[a], Pascal Wong-Wah-Chung[a].

[a] Aix Marseille Univ, CNRS, LCE, Marseille, France

[b] Université Clermont Auvergne, CNRS, UMR 6296, Université Blaise Pascal, Institut de Chimie de Clermont-Ferrand (ICCF), 8 Avenue Blaise Pascal, TSA 60026, CS 60026, 63178 Aubière cedex, France

Corresponding author:
Stéphanie Rossignol: Aix-Marseille Université, LCE, Europôle de l'Arbois, bat. Villemin, BP80, 13545 Aix-en-Provence- France
Tel: 00 33 4 42 90 84 02; Fax: 00 33 4 13 55 10 60
Stephanie.rossignol@univ-amu.fr

S1: OPC 1.109 - 31 channels
0.25/ 0.28/ 0.3/ 0.35/ 0.4/ 0.45/ 0.5/ 0.58/ 0.65/ 0.7/ 0.8/ 1.0/ 1.3/ 1.6/ 2/ 2.5/ 3/ 3.5/ 4/ 5/ 6.5/ 7.5/ 8.5/ 10/ 12.5/ 15/ 17.5/ 20/ 25/ 30/ 32/ > 32 µm.

S2: Infrared spectrum of pristine and UV aged virgin PE, acquired in transmission mode from 400 to 4000 cm^{-1} using a Nicolet 6700 Thermo Scientific infrared spectrophotometer.

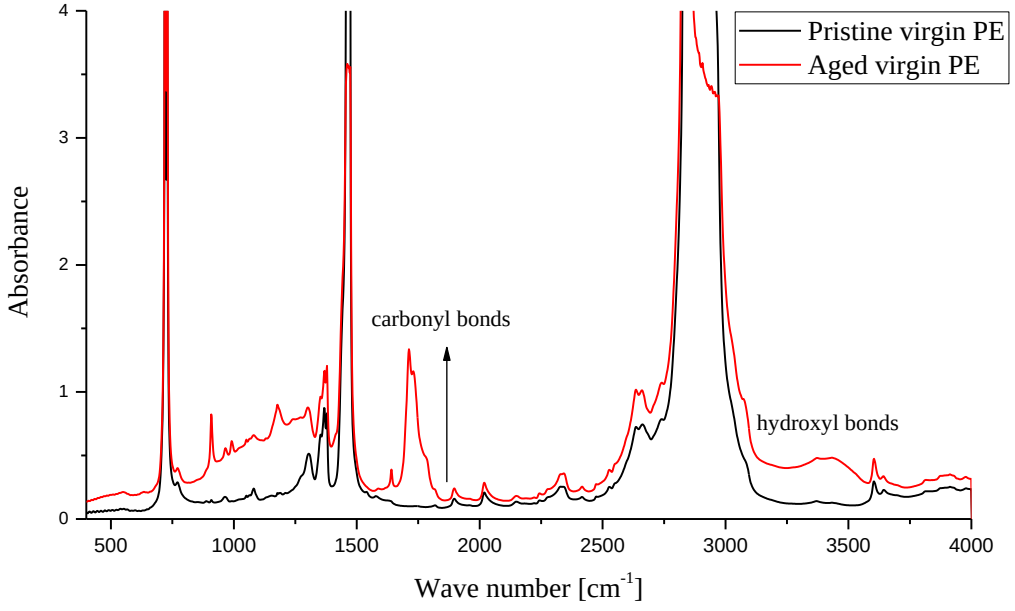

S3: Infrared spectrum of pristine and UV aged formulated PE, acquired in transmission mode from 400 to 4000 cm^{-1} using a Nicolet 6700 Thermo Scientific infrared spectrophotometer.

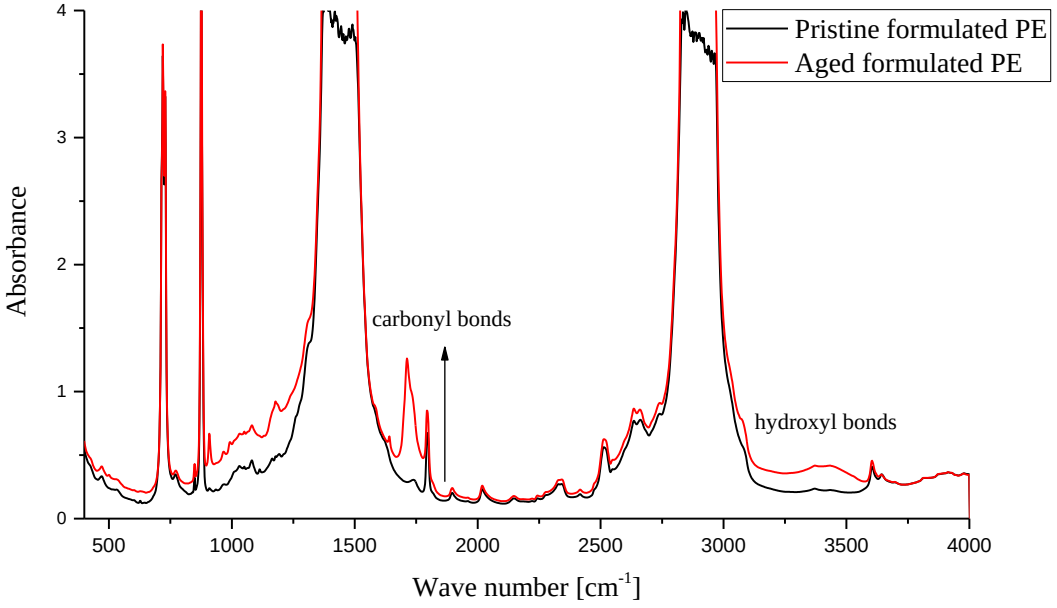

S4: Normalized mean particle size distribution for the background signal, and two concentration levels in ultrapure water of (A) PE_{Nano} (200 - 9900 nm) and (B) PS (350 nm) measured by the OPC. For each particle type, two concentration levels were tested (C1 and C2). For PS 350, 5 initial drops were added followed by 5 more drops 30 min after the first addition. For PE_{Nano}, 25 mg were suspended in water were initially added, followed by 25 mg 30 min after the first addition.

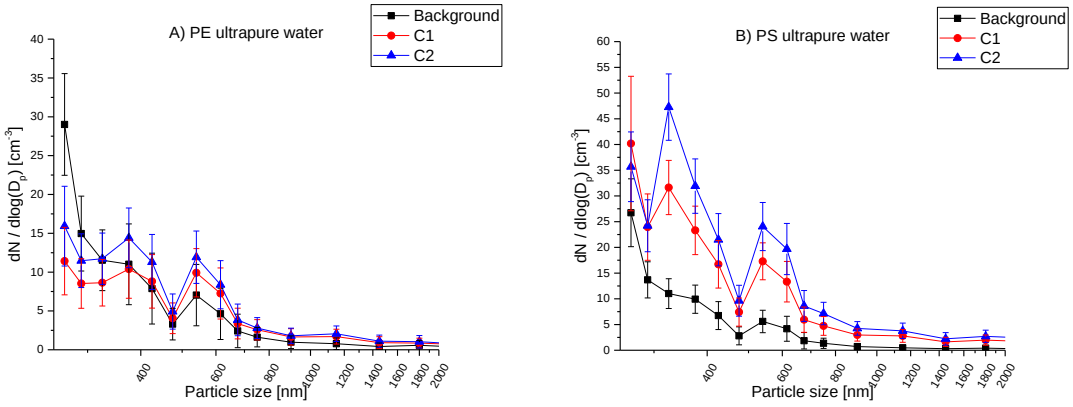

S5: EDX analysis of the layer surrounding the PS agglomerates presented in figure 5-D.

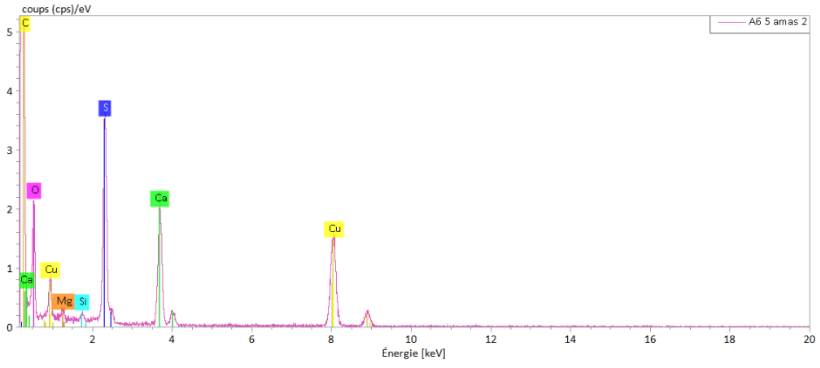

S6: Evolution of the normalized particle concentration measured in the 300 - 350 nm channel of the OPC for PS 350 nm and PE_{Nano} in water with 0.43 µM SDS as a function of time.

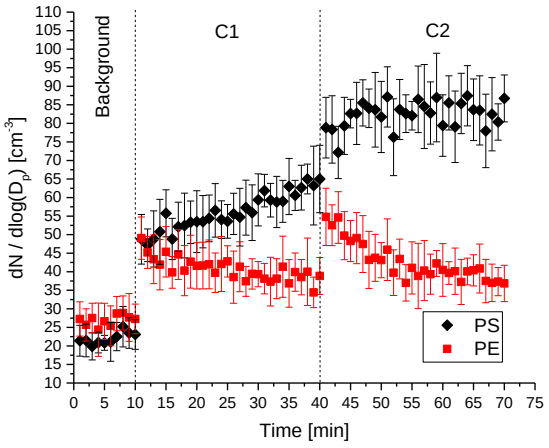

S7: Normalized mean particle size distribution measured by the OPC for PS 350 nm and PE_{Nano} with different generated bubble sizes. For clarity purpose, particles concentrations measured with SDS solution only was used as background signal and subtracted from the signal generated following particle addition, an average of 10 min for each being considered.

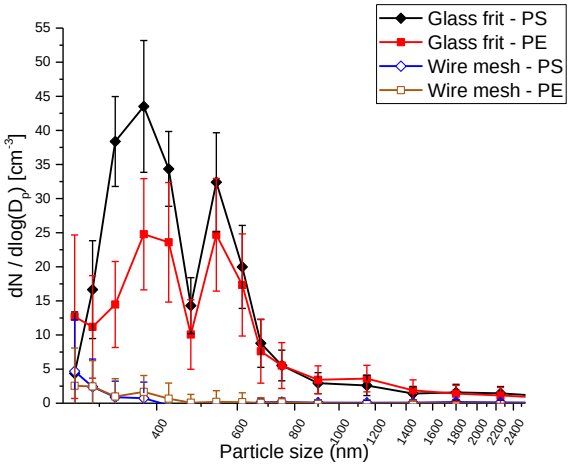

S8: Behaviour of UV aged virgin PE showing an increase then stabilization after particle addition.